Chemical Engineering Journal 106 (2005) 197–211

Chemical Engineering Journal

www.elsevier.com/locate/cej

Flow behavior of clusters in a riser simulated by direct simulation Monte Carlo method

Wang Shuyan[a], Liu Huanpeng[a], Lu Huilin[a,*], Liu Wentie[a], Jiamin Ding[b], Li Wei[a]

[a] *School of Energy Science and Engineering, Harbin Institute of Technology, Harbin 150001, China*
[b] *Agere Systems Inc., 555 Union Boulevard, Allentown, PA 18109, USA*

Received 18 September 2004; received in revised form 26 November 2004; accepted 2 December 2004

Abstract

A discrete particle motion-collision decoupled model has been developed based on gas molecular dynamics and gas–solid two-phase fluid dynamics. Particle collision is modeled by means of the direct simulation Monte Carlo (DSMC) method. The Newtonian equations of motion are solved for each simulated particle in the system. The interaction between gas phase and simulated particle is determined by means of Newtonian third law. The flow behavior of gas and particles phases were numerically simulated in a circulating fluidized bed. The distributions of gas and particle velocity and particle concentration in the risers were analyzed. The duration time, averaged solid concentration in cluster, the ratio of total cluster duration time to total observation time and the cluster frequency were obtained in the circulating fluidized bed. The simulated results are in agreement with experimental measurements by Manyele et al. [S.V. Manyele, J.H. Parssinen, J.X. Zhu, Characterizing particle aggregates in a high-density and high-flux CFB riser, Chem. Eng. J. 88 (2002) 151–161] and Sharma et al. [A.K. Sharma, K. Tuzla, J. Matsen, J.C. Chen, Parametric effects of particle size and gas velocity on cluster characteristics in fast fluidized beds, Powder Technol. 111 (2000) 114–122] in the circulating fluidized beds. The wavelet multi-resolution analysis was used to analyze the simulated data of instantaneous particle concentration. From the random-like particle concentration fluctuations, the cluster frequency can be extracted based on the wavelet multi-resolution analysis over a time–frequency plane.

Keywords: DSMC method; Discrete particle motion-collision decoupled model; Clusters

1. Introduction

Circulating fluidized beds are widely used in the petroleum, chemical, metallurgical and energy industries. In the last decade, significant research efforts have been made to develop detailed microbalance models to study the complex hydrodynamics of circulating fluidized beds. Broadly speaking the simulation approaches of two-phase flow in circulating fluidized bed can be classified into Euler–Euler two-fluids model and Euler–Lagrange discrete particle trajectory model. In two-fluids models, gas and solid phases are both considered as continuous mediums, and balance equations of each phase are established to investigate the flow behavior of gas and solid phases. The models predicted well the bubble formation and the distribution of time-averaged solids concentration in bubbling fluidized beds (e.g. [1–5]), and hydrodynamic of gas and particles phases in circulating fluidized beds (e.g. [6–13]). On the contrary, in the Euler–Lagrange particle trajectory model, gas is considered as the continuous medium and the motions of particles are treated in the Lagrange coordinate by solving the motion equations. In general, particle–particle collisions can be neglected in the simulation of dilute gas–solid two-phase flows. However, the effect of particle–particle collision on the flow behavior must be considered in the simulation of gas–solid two-phase flows in circulating fluidized beds. Several attempts have been made to simulate gas-particle fluidization using the discrete element method (DEM). In this method, the mechanism of particle–particle collisions has been described by

* Corresponding author.
E-mail address: huilin@hit.edu.cn (L. Huilin).

1385-8947/$ – see front matter © 2004 Elsevier B.V. All rights reserved.
doi:10.1016/j.cej.2004.12.036

Nomenclature

C_{d0}	drag coefficient
C_v	constant
d	particle diameter
e	coefficient of restitution
f_c	collision frequency of particles
f_d	drag force
F	time fraction
g	gravity
g_o	radial distribution function
G_s	solid mass flux
h	height of riser
I	unit vector
m	particle mass
n	particle number density
p	fluid pressure
p_{ij}	collisional probability
r	position, distance from walls
R	random number, radii of riser
s	local area of a particle
t	time, tangential unit vector
u_g	gas velocity, superficial gas velocity
v	particle velocity
x	location along lateral direction
y	location along vertical direction

Greek symbols

ε	porosity
ε_s	solid concentration
μ	dynamic friction coefficient
$\mu_{lam,g}$	laminar viscosity of gas phase
μ_f	coefficient of tangential restitution
μ_t	turbulent viscosity of gas
θ	granular temperature
ρ_g	gas density
ρ_s	particle density
σ	standard deviation
τ_g	gas stress tensor
ω	rotational velocity of particles

Subscripts

g	gas phase
i	index of particle
n	normal direction
s	particles
t	tangential direction

soft-sphere models as well as hard-sphere models. Hoomans et al. [14] presented a hard-sphere approach where collisions are assumed to be binary and instantaneous. Xu and Yu [15] developed a hybrid technique combining elements of both soft-sphere and hard-sphere techniques. Hard-sphere model uses the coefficient of restitution and friction coefficient as an input. Flow patterns of bubbling, slugging and particle cluster motions in fluidized beds were simulated using hard-sphere model [14–18]. In the soft-sphere models, the collisions between particles are simulated by Hooke's linear springs and dashpots. It uses the spring constant, damping coefficient and friction coefficient as an input. This model has been used for investigation of the effect of interparticle force on fluidization characteristics [19,20], the effect of internals on fluid dynamics [21], and the effect of pressure and temperature on fluidized bed behavior [22,23].

Direct simulation Monte Carlo (DSMC) method is widely used in the simulation of rarefied gas [24]. Each simulated particle represents many physical particles in the DSMC method. The position coordinates of simulated particles change continuously due to particle motion and collisions. Macroscopic parameters, such as the distribution of velocity and concentration of particles, can be obtained from all simulated particles in the cell. When the inertia force dominates the drag force, particle motion in circulating fluidized beds is well described by the impulsive equations of motion in which collisions against another particle are assumed to occur instantaneously. Therefore, the motion of particle in the circulating fluidized bed is similar to that of molecules in rarefied gas except that the kinetic energy of particle fluctuating motion tends to decay by the inelastic and frictional aspects of collision [25]. Hence, the DSMC method can be used to simulate the particle motion in the circulating fluidized bed. Yonemura and Tanaka [26] investigated the formation of clusters in the circulating fluidized bed by means of DSMC method. Effects of physical properties of particles on the structure of particle clusters were studied numerically in a rectangular domain with periodic boundaries [27]. A numerical simulation was performed for a dispersed gas–solid flow in a vertical channel by DSMC method [28]. It is found that the flow becomes unstable and inhomogeneous as the gas velocity decreases and the solid loading increases. The V-shaped and reverse V-shaped clusters were predicted by Tsuji et al. [29] in the circulating fluidized bed by means of DSMC method. The expansion behavior and structural phenomena of fluid–particle systems was simulated using the Monte Carlo method in the fluidized bed [30]. The model of probability of particle collisions was proposed based on the change in the system's potential energy and the average kinetic energy of the system. DSMC method was used to predict particle motions in a group-B particle turbulent fluidized bed [31]. The complex bubbling flow and the particle cluster formation were predicted in the fluidized bed.

In this study, the locally averaged Navier–Stokes equations of gas phase and Lagrangian type particle motion equations, where the mutual interactions between gas phase and particles and the particle collisions are taken into account, were simultaneously solved. Particle collision is modeled by means of the direct simulation Monte Carlo (DSMC) method. The Newtonian equations of motion are solved for each simulated particle in the system. The distributions of velocity and

concentration of particles in the riser were analyzed. The duration time, averaged solid concentration in cluster, the ratio of total cluster duration time to total observation time and the cluster frequency were obtained in the circulating fluidized bed. The simulated results are compared with experimental findings. The wavelet multi-resolution analysis is used to investigate the flow behavior of clusters based on the simulated data of instantaneous particle concentrations. From the random-like particle concentration fluctuations, the cluster frequency was determined from the wavelet multi-resolution analysis over a time–frequency plane.

2. DSMC method

The DSMC method is a trajectory method, which makes it possible to deal with interparticle collision based on sample particles that the number of which is smaller than the actual number of particles. In the DSMC, a sampled particle motion is dissolved into the movement and collision processes. Simulated particle movement obeys the single particle motion model, and the collision process follows the particle collisional dynamics. The computation procedure of particle motion and collision decouple model is as follow [24,29]:

(1) Position of a sampled particle is determined by solving the single particle motion equation in a time step small enough without considering the particle–particle collisions.
(2) Particle–particle collision is calculated by means of Monte-Carlo method. If particle i collides with particle j in the time step, the post-collision velocities of particles are calculated by the collisional dynamics. The particle velocities are replaced by the post-collision velocities, but without changing them positions.

The collision probability of particle i during a time step Δt is given by:

$$P_i = \sum_{j=1}^{N} P_{ij} \tag{1}$$

where N is the number of simulated particles in the cell. In the high concentration of particles, the dense packing effect on the collision frequency of particles was considered. The modified collision probability of simulated particle i and j is [24,29]:

$$P_{ij} = \frac{n}{N}\pi d^2 g_o u_{ij} \Delta t \tag{2}$$

where n is local particle number density, d particle diameter, and u_{ij} relative velocity between particle i and j, Δt is time step. In above equation, the radial distribution function at contact, g_o, was introduced, as done with the factor χ in kinetic theory of gases by Chapman and Cowling [32]. Hence, the radial distribution function is applied to correct the probability of a collision for the effect of the volume occupied by the particles. The value of radial distribution function at contact was calculated as follows [33]:

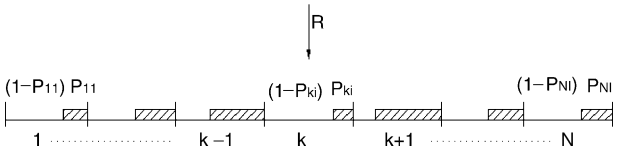

Fig. 1. Modified Nanbu method.

$$g_o(\varepsilon_s) = \left[1 - \left(\frac{\varepsilon_s}{\varepsilon_{max\,s}}\right)^{1/3}\right]^{-1} \tag{3}$$

where the maximum packed solids fraction $\varepsilon_{max\,s}$ of 0.63 was used in the simulations.

Several schemes to search collision pairs with the use of the Monte Carlo Method have been proposed, such as the time counter method, the Nanbu method and the modified Nanbu method [24]. The modified Nanbu method is used in this study. The procedure is as follows. Seeing Fig. 1, a random number R is extracted from a generator, which has a uniform distribution ranging from zero to unity. A candidate collision partner k in a computation cell is selected in the time step Δt using the equation:

$$k = \text{int}[R \times N] + 1 \tag{4}$$

where [ ] is defined as the integer part of $(R \times N)$. If the relation

$$R > \frac{k}{N} - p_{ki} \tag{5}$$

is satisfied, it is decided that particle i collides with particle k during the time step Δt, and the velocity of particle i is replaced by the post-collisional velocity. The relative position between particle i and particle k after collision can be determined. Otherwise, the collision does not happen in this time step.

In order to decrease the computer capacity efficiently in the simulations, the sub-cell method is applied [24]. The computing field is divided into several gas cells. A gas control cell is also divided into several sub-cells, seeing Fig. 3. The search for a collision partner is carried out in the sub-cells, and the interaction between gas and particle phases is calculated in a gas control cell. With this method the collision partner can be more efficiently determined.

3. Eulerian–Lagrangian gas–solid flow model

3.1. Continuity and momentum equations for gas phase

The Euler–Lagrangian method computes the Navier–Stokes equation for the gas phase and the motion of individual particles by the Newtonian equations of motion. For the gas phase, we write the equations of conservation of mass and momentum [34]:

$$\frac{\partial}{\partial t}(\rho_g \varepsilon_g) + \nabla \cdot (\rho_g \varepsilon_g \boldsymbol{u}_g) = 0 \tag{6}$$

$$\frac{\partial}{\partial t}(\varepsilon_g \rho_g \boldsymbol{u}_g) + \nabla \cdot (\varepsilon_g \rho_g \boldsymbol{u}_g \boldsymbol{u}_g) = -\varepsilon_g \nabla P - S_{p-g} - (\nabla \cdot \tau_g) + \varepsilon_g \rho_g \boldsymbol{g} \tag{7}$$

$$\tau_g = \mu_g [\nabla \boldsymbol{u}_g + \nabla \boldsymbol{u}_g^T] - \tfrac{2}{3}\mu_g \nabla \cdot \boldsymbol{u}_g \boldsymbol{I} \tag{8}$$

$$\mu_g = \mu_{lam,g} + \mu_t \tag{9}$$

where u_g and ρ_g are gas velocity and density, respectively. ε_g is the void fraction. S_{p-g} is the interaction drag force acting on a particle. The interaction forces between the two phases should be equal and have reverse directions. The value can be determined by:

$$S_{p-g} = \frac{\sum_{i=1}^{N} f_{d,i}}{S} \tag{10}$$

Yuu et al. [35] has modeled turbulent viscosity coefficient of subgrid-scale turbulence caused by the subgrid-scale fluctuations using large eddy simulation (LES) in which the effect of particle oscillations on gas turbulence has been taken into account. The turbulent viscosity of gases is as follows:

$$\mu_t = C_v \Delta \rho_g k_g^{1/2} \tag{11}$$

where, $\Delta = (\Delta x \Delta y)^{1/2}$, and $k_g = \frac{1}{2}\overline{u}'_{gx}\overline{u}'_{gy}$ is gas turbulent energy. The model of gas turbulent energy proposed by Yuu et al. [35] is used in this simulation.

3.2. Particle motion equations

The particle motion is subject to Newton's equation of motion. Magnus force, Saffman force, Basset, and the unsteady force are neglected due to the high ratio of particle density to gas density. The equation of translational motion of a particle can be written as follows [14,17]:

$$m\frac{dv_i}{dt} = -\frac{\pi}{6}d_i^3 \nabla p + f_d + m_i g \tag{12}$$

$$f_d = \left(\frac{1}{16}\right) C_{d0,i} \rho_g \pi d_i^2 |u_{gi} - v_i| (u_{gi} - v_i) \varepsilon_g^{-\delta} \tag{13}$$

where the drag force coefficient $C_{d0,i}$ is written as:

$$C_{d0,i} = \left(0.63 + \frac{4.8}{Re_{p,i}^{0.5}}\right)^2 \tag{14}$$

$$Re_{p,i} = \rho_g d_i \frac{|u_{gi} - v_i|}{\mu_g} \tag{15}$$

$$\delta = 3.7 - 0.65 \exp\left[-\frac{(1.5 - \log_{10} Re_{p,i})^2}{2}\right] \tag{16}$$

The equation of rotational motion of a particle is written as:

$$\frac{m_i d_i^2}{10}\frac{d\omega_i}{dt} = \frac{\rho_s d_i^2}{64}\left(\frac{6.45}{Re_\omega} + \frac{32.1}{Re_\omega}\right)|\omega_i|\omega_i \tag{17}$$

where $Re_\omega = d_i^2 \rho_g |\omega| / (4\mu_g)$.

3.3. Particle collision dynamics

Analysis of particle's collision in this study is based on collision dynamics with the following assumptions: (1) particles are spherical and quasi-rigid. (2) Interaction forces are impulsive and all other infinite forces are negligible during collision. (3) Particle motion is two-dimensional with the particle mass center moving in one plane. The changes of velocity after a collision between two particles with the same diameter and mass are subject to the following equations [14,17,18]:

$$m_i(v_{i,1} - v_{i,0}) = J \tag{18}$$

$$m_j(v_{j,1} - v_{j,0}) = -J \tag{19}$$

$$\frac{m_i d_i^2}{4}(\omega_{i,1} - \omega_{i,0}) = n \times J \tag{20}$$

$$\frac{m_j d_j^2}{4}(\omega_{j,1} - \omega_{j,0}) = -n \times J \tag{21}$$

where, $v_{i,0}$ and $v_{j,0}$ represent the pre-collisional velocities of particle i and particle j, respectively. $v_{i,1}$ and $v_{j,1}$ represent the post-collisional velocities of particle i and particle j, respectively. n is the normal unit vector between particle i and j. The relative velocity between the two colliding particles is defined as:

$$v_{ij} = (v_{i,c} - v_{j,c}) \tag{22}$$

The normal and tangential components of the impulse vector calculated by coefficient of restitution e and friction coefficient μ_f are written as:

$$J_n = -\frac{(1+e)m_i m_j}{(m_i + m_j)}(v_{ij,0} \cdot n) \tag{23}$$

$$J_t = -\mu_f J_n \tag{24}$$

The total impulse vector is defined as:

$$J = J_n n + J_t t \tag{25}$$

$$t = \frac{v_{ij,0} - n(v_{ij,0} \times n)}{|v_{ij,0} - n(v_{ij,0} \times n)|} \tag{26}$$

3.4. Grid mapping

For the calculation of the force acting on a suspended particle, local averaged values of pressure, porosity and velocity of gas at the position of the particle (the Lagrangian grid) are required. Due to the numerical solution method used, these variables are only known at discrete nodes of the computational domain. An area weighted averaging technique is used

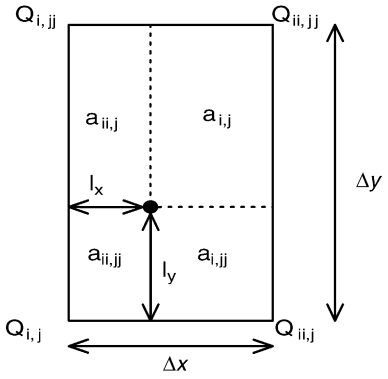

Fig. 2. Calculation method of local parameters.

to obtain the local averaged value $\bar{Q}$ of a quantity $Q(i, j)$ from the four surrounding computational nodes, seeing in Fig. 2. The local averaged value can be calculated as follows:

$$\bar{Q} = \frac{a_{i,j}Q_{i,j} + a_{ii,j}Q_{ii,j} + a_{ii,jj}Q_{ii,jj} + a_{i,jj}Q_{i,jj}}{\Delta x \Delta y} \quad (27)$$

where, $a_{i,j} = (\Delta x - l_x)(\Delta y - l_y)$, $a_{ii,j} = l_x(\Delta y - l_y)$, $a_{ii,jj} = l_x l_y$, $a_{i,jj} = l_y(\Delta x - l_x)$.

3.5. Calculation of porosity

For each cell of the computational domain, porosity can be calculated on the basis of the area occupied by the particles in the cell. The porosity is obtained by subtracting the sum of the particle volumes from the volume of a fluid cell. When a particle overlaps one neighboring cell or more, the volume fraction included in a particular fluid cell is taken into account to calculate the porosity of the cell. A "2D" porosity in the cell is defined as:

$$\varepsilon_{g,2D} = 1 - \frac{\sum_{i=1}^{n} s_i}{\Delta x \Delta y} \quad (28)$$

where Δx and Δy are the width of computational cell, and s is the surface area of the particle located in the cell. However, the above-defined "2D" porosity is inconsistent with the applied empiricism in the calculation of the drag force exerted on a particle and of the interfacial friction, since the relevant correlations are from 3D systems. In order to be more consistent, we used a 3D porosity $\varepsilon_{g,3D}$ as[16]:

$$\varepsilon_{g,3D} = 1 - \frac{2}{\sqrt{\pi\sqrt{3}}}(1 - \varepsilon_{g,2D})^{3/2} \quad (29)$$

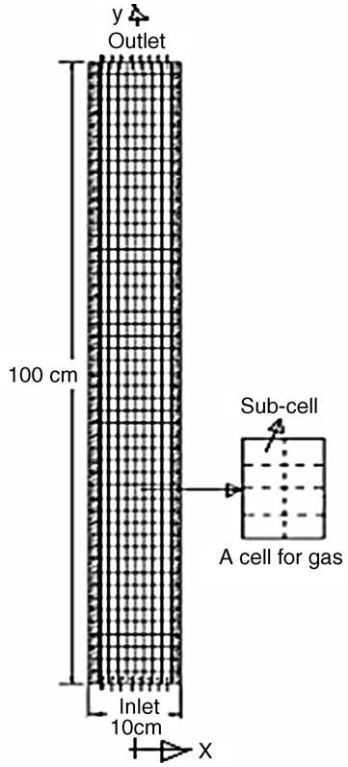

Fig. 3. Grid arrangement for simulation in the two-dimensional riser.

3.6. Initial and boundary conditions

Fig. 3 shows the two-dimensional riser section used in the present numerical simulation of gas–solids flow. The computational parameters are listed in Table 1. Initially, the velocities of gas and particles phases were set at zero in the riser. Inlet gas pressure, gas velocity and particle velocity are given. Uniform bottom-inlet conditions are assumed. A no-slip condition is used for gas phase at the walls. The rotational velocity of particles was set at zero at the walls. The particle velocity after it rebounds from the wall can be determined by:

$$v_{i2} = -e_n(v_{i1}) \quad \text{and} \quad u_{i2} = -e_t(u_{i1}) \quad (30)$$

Table 1
Parameter used in simulations

Particle shape	Sphere	Number of entering particles	100,0000 (1/s)
Particle diameter	0.1 (mm)	Number of real particle/simulated particle	100
Particle density	1700 (kg/m^3)	Height of riser	1 (m)
Restitution coefficient of particles	0.9	Diameter of riser	0.08 (m)
Coefficient of restitution between particle and wall	0.9	Temperature	300 (K)
Tangential restitution coefficient	0.3	Superficial gas velocity	4.9 (m/s)
Friction coefficient	0.1	Grid number (*nx*, *ny*)	40, 150
Gas viscosity	1.5×10^{-5} (Pa s)	Gas density	1.2 (kg/m^3)

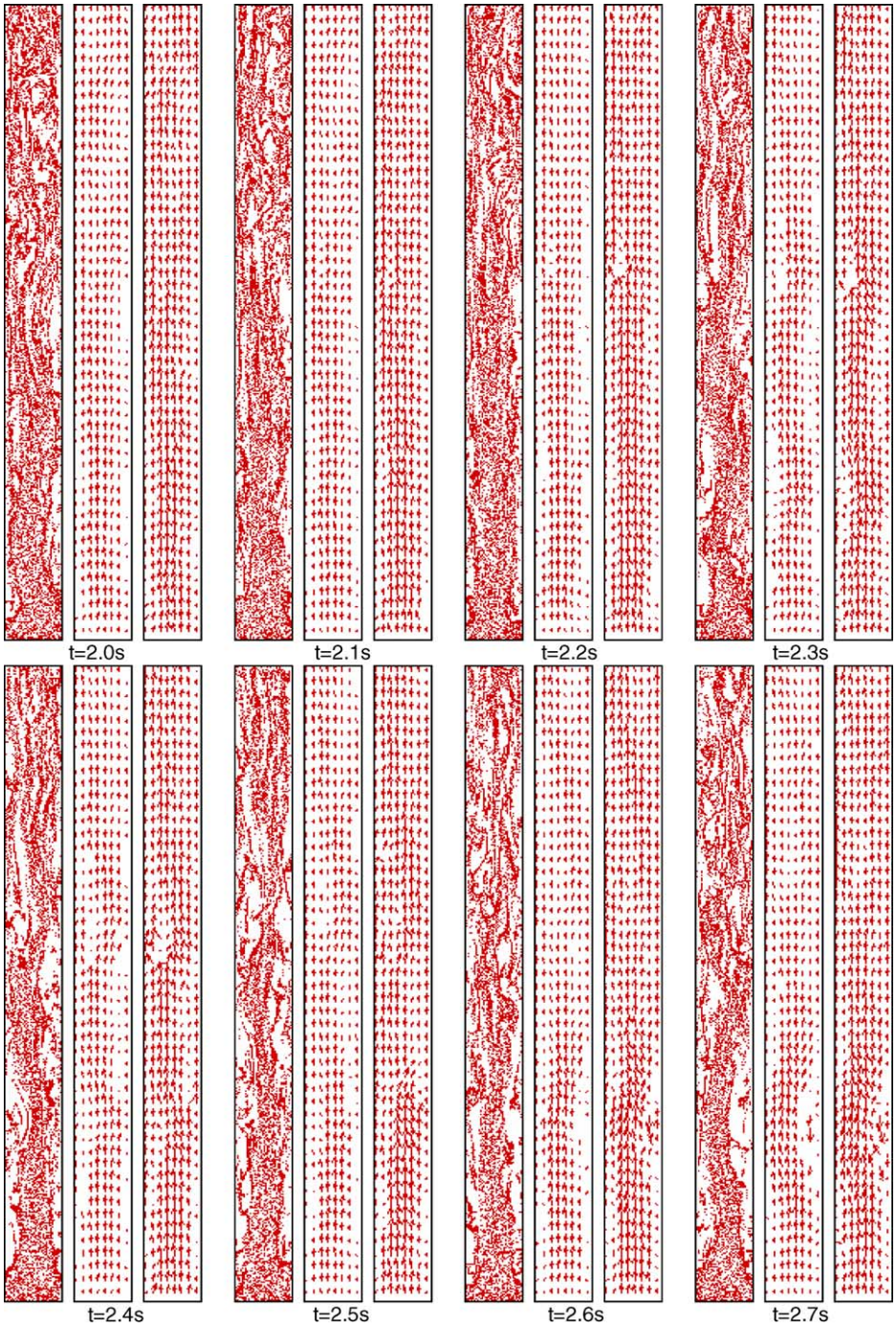

Fig. 4. Motions of particles in the circulating fluidized bed (right, particle concentration; middle, gas velocity; left, particle velocity).

where e_n and e_t are two restitution coefficients in the normal and tangential directions, respectively. In accordance with Jun and Tabako [36], the restitution coefficients can be determined in terms of the particle impact angle as follows:

$$e_t = 1 - 2.12\beta + 3.0775\beta^2 - 1.1\beta^3 \quad \text{and}$$
$$e_n = 1 - 0.4159\beta + 0.4994\beta^2 - 0.292\beta^3 \tag{31}$$

where the impact angle, β, is in radian.

4. Result and discussions

Fig. 4 shows a snapshot of simulation representing vertical cross-section images, velocity vector of gas and particles phases as a function of times at the superficial gas velocity of 4.9 m/s. The snapshots show representative cluster structures in the riser. From these figures, the forms of clusters with a local high particle concentration are observed. The formation, movement and breaking of clusters appeared continuously

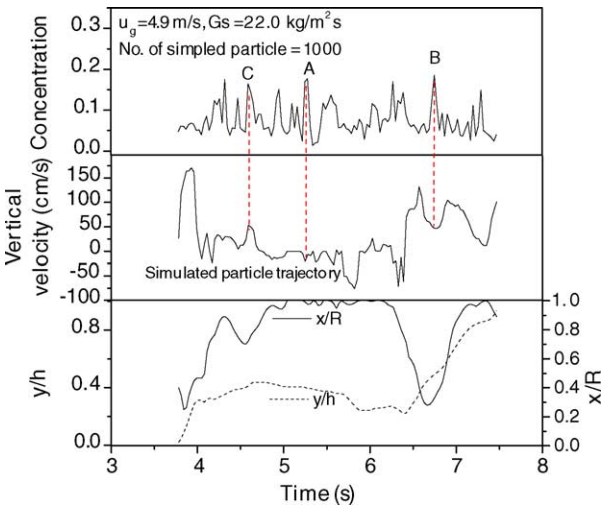

Fig. 5. Variations of instantaneous vertical velocity, concentration and positions of simulated particle.

in the riser. The clusters move upward or downward companying with the formation and disjointing of clusters. The negative values of the instantaneous axial velocities of particles indicate the descending motion toward to the bottom. The formations of particle clusters begin to develop due to some kind of perturbation in the system. Once developed, the particle clusters capture the isolated particles in its front and leave a more dilute zone in its tail. In this way, the cluster increases in size and a dense cluster is formed [17]. Such cluster structures have been experimentally observed by Van Den Moortel et al. [37] using the laser sheet technique, obtained from numerical simulations by Ito et al. [38] using a direct simulation Monte Carlo method, and by Helland et al. [17] using a hard-sphere discrete particle model. Van Den Moortel et al. [37] found that the up-flowing particle clusters exhibit a horseshoe shape heading upwards with thin downward tails. Simulation results show that the particle clusters move with axial velocities from 0.1 to 2.0 m/s. Fig. 5 shows the instantaneous positions and vertical velocity of simulated particle, and the concentration of particles located in the cell as a function of time in the riser. The simulated particle was accelerated when it was captured by the downward cluster, and decelerated as it was left from the downward cluster (e.g. at point A). However, the simulated particle was decelerated when it was captured by the upward cluster and accelerated as it was left from the upward cluster (e.g. at point B). Helland et al. [17] pointed out that the life of a cluster can be described in three periods: a formation phase, an established phase and a decaying phase. During the cluster formation, the particle phase is accelerated and simultaneously, the gas phase is decelerated due to the two-way coupling between the gas and particle phases, thus a decrease in their relative velocity. In the established phase, the velocity of the dense cluster as a unit is found to be constant. In the decaying phase, the cluster may vanish in the form of particles following their own trajectories, or it may take a part of a new cluster. This process has been observed at point C in Fig. 5 from simulated particle trajectory.

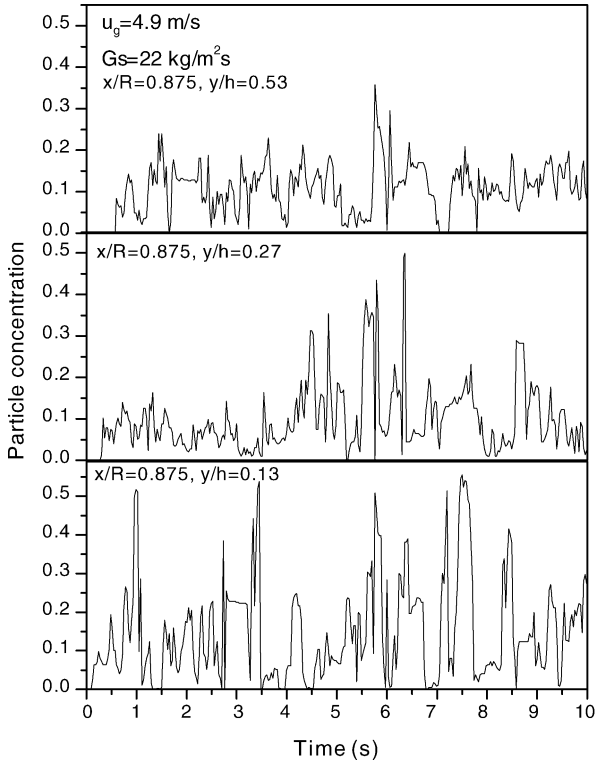

Fig. 6. Particle concentration fluctuation near the wall.

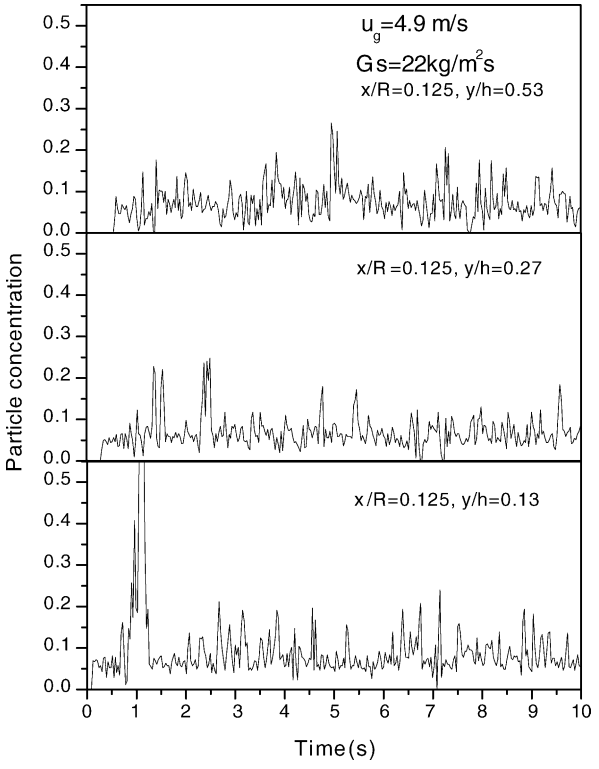

Fig. 7. Particle concentration fluctuation in the center.

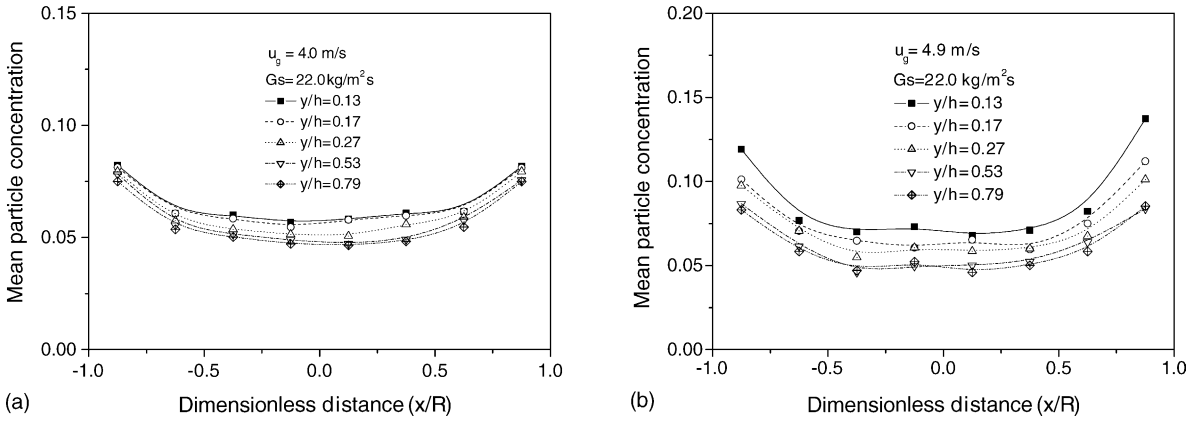

Fig. 8. Distribution of time-averaged particle concentrations.

Figs. 6 and 7 show the instantaneous particle concentrations near the wall and at the center at the superficial gas velocity of 4.9 m/s. A high instantaneous concentration of particles means the occurrence of clusters, and the low concentration indicates the motions of dispersed particles. It can be seen that the concentration fluctuates more strongly near the wall than that at the center. This indicates that the clusters are formed near the wall regime. Fig. 8a and b show the distribution of time-averaged concentration of particles phase at the different height at the superficial gas velocity of 4.0 and 4.9 m/s, respectively. The particle concentration decreases along the height. The core-annulus structure can be observed with a denser zone close to the walls and a dilute zone in the center. Tsukada et al. [39] stated that the wall down flow behaves as a collector of clusters diffused from the core region.

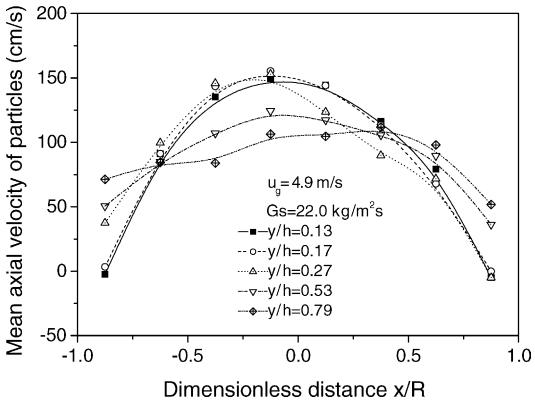

Fig. 10. Distribution of mean axial velocity of particles.

Fig. 9 shows the fluctuations of instantaneous axial and lateral particle velocities near the wall and at the center at the superficial gas velocity of 4.9 m/s. The oscillating particle velocity is stronger at the center than that near the wall because of the effect of gas turbulent flow. At the wall region, the positive or negative lateral velocities of particles mean particles move along the transversal direction from the wall to center, or versus. The distributions of time-averaged axial velocity of particles are shown in Fig. 10 at the superficial gas velocity of 4.9 m/s. The time-averaged axial velocity of particle is lower near the walls than that at the center. From Fig. 9, we observe the large-scale fluctuations around a mean value of particle velocity. The histograms of axial and lateral particle velocities are shown in Fig. 11. The mean values of particle velocity

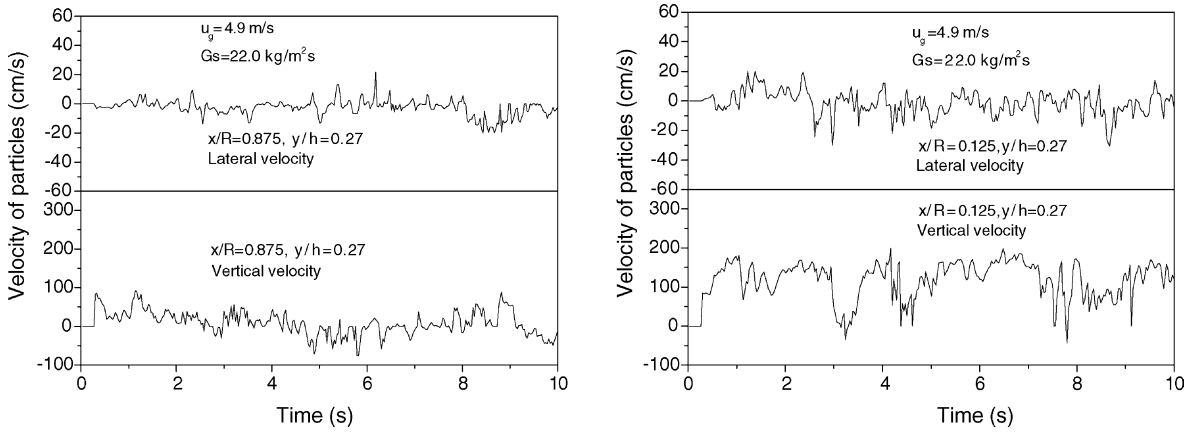

Fig. 9. Instantaneous lateral and vertical velocity of particles near the walls and at the center of riser.

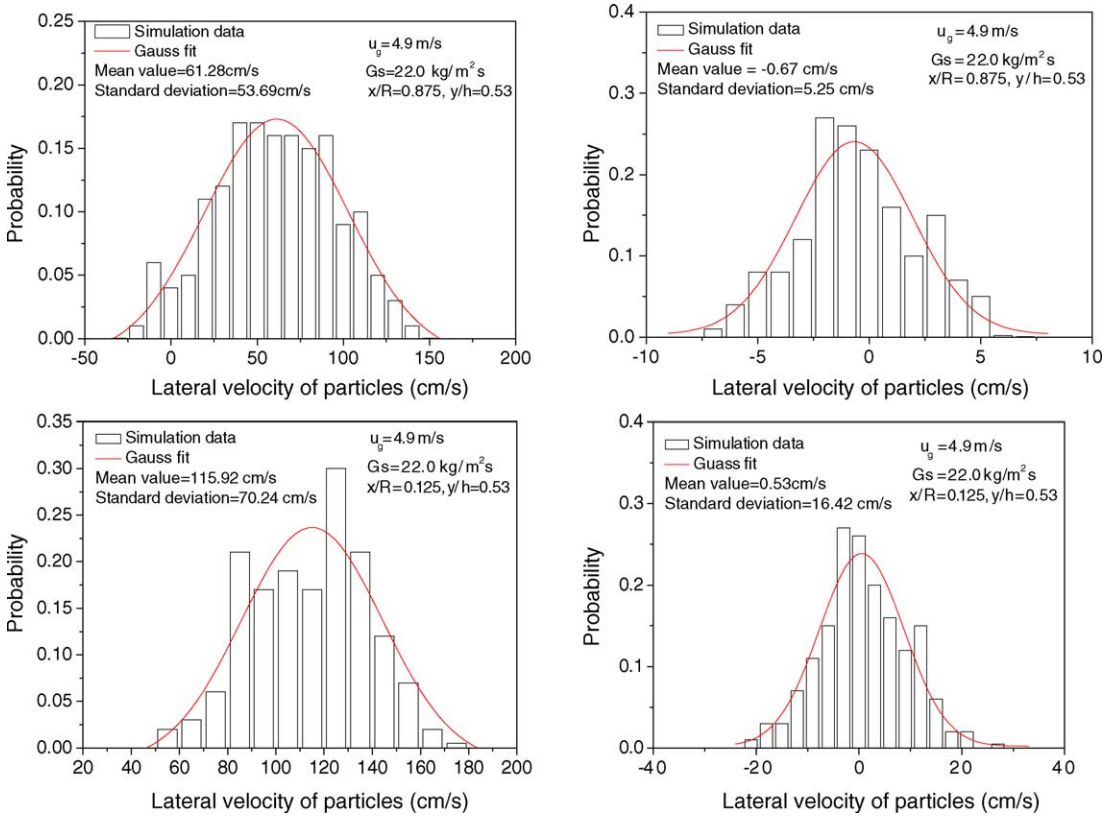

Fig. 11. Histogram of lateral and axial velocity of particles.

and standard deviation, $\sigma = \sqrt{1/(N-1)\sum_{i=1}^{N}(v_i - v_m)^2}$, are also indicated in the figures, where v_m is a mean velocity, v_i is a instantaneous velocity of particles. From these figures, we see that the axial and lateral velocities of particles can be fitted by the Gaussian distribution. The standard deviations of vertical velocity are always larger than that of lateral velocity of particles. Such anisotropic flow of particles has been experimentally observed by Gidaspow and Huilin [40] in the riser. The presence of clusters is the predominant effect of this fluctuating behavior. The granular temperature, θ, defined as a measure of particle fluctuations can be obtained from the histogram of particle velocity [40]:

$$\theta = \left(\frac{1}{3}\sigma_y^2 + \frac{2}{3}\sigma_x^2\right) \tag{32}$$

Fig. 12 shows the computed granular temperature as a function of particle concentration in the riser. The computed granular temperature increases, reaches a maxima, then decreases with the increase of particle concentration. When the particle concentration closes to the packing, the granular temperature approaches to zero, since particles can hardly move. Similar trends were also found from numerical simulations by Neri and Gidaspow [8] and Huilin et al. [12] using Euler–Euler two-fluid model with kinetic theory of granular flow.

Using DSMC method, the collisional frequency of particles was obtained. Fig. 13 shows the profile of the collisional frequency of particles as a function of particle concentration at the superficial gas velocity of 4.9 m/s. We see that the computed collisional frequency increases with the increase of particle concentration. The lower the particle concentrations, the less the collisional frequency of particles. In the molecular simulation, the collision probability was calculated by Eq. (2) without considering the radial distribution function ($g_o = 1.0$). The probability of collision between two simulated molecules over the time internal is proportional to the product of their relative speed and the total cross-section, and its

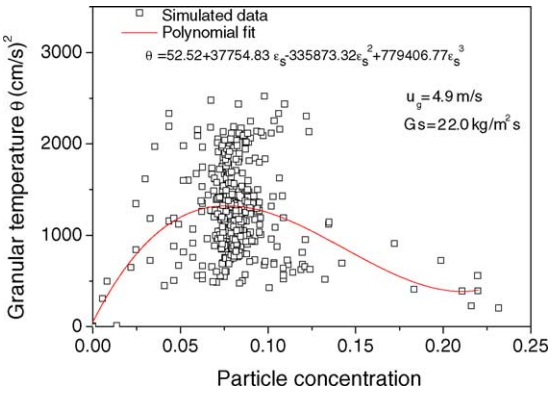

Fig. 12. Relation between granular temperature and particle concentrations.

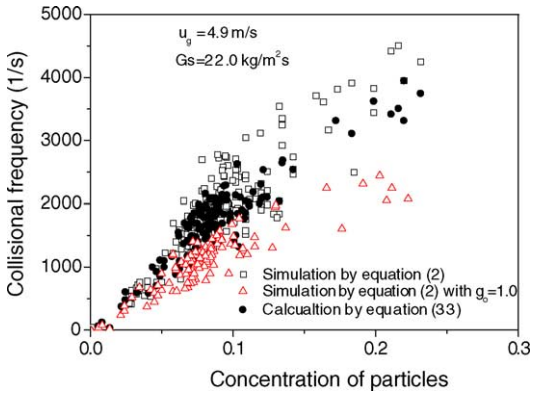

Fig. 13. Profiles of particle collision frequency as a function of concentration of particles.

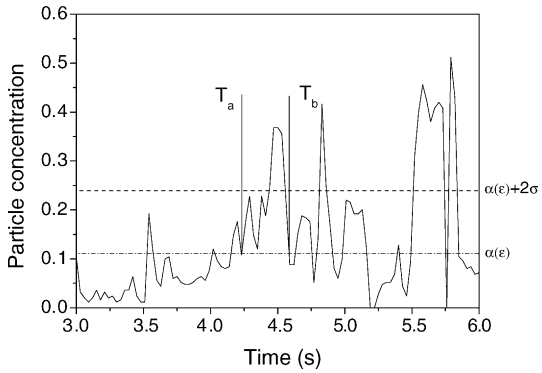

Fig. 14. Determination of a cluster formation.

value can be calculated from Eq. (2) with $g_o = 1.0$ ([24,29]). The predicted particle collision frequency using Eq. (2) with $g_o = 1.0$ was shown in Fig. 13. Simulated results showed that the particle collision frequency was lower with $g_o = 1.0$ than that using Eq. (2). In the low concentration of particles, the calculated collision frequency of particles is close each other, since the radial distribution function is close to unity. However, the difference is evident at the high concentration of particles.

Based on the kinetic theory of granular flow the collisional frequency per unit volume can be calculated as follows [34]:

$$f_c = 6.77\left(\frac{\varepsilon_s}{d}\right) g_o \sqrt{\theta} \tag{33}$$

The collisional frequency of particles calculated from Eq. (33) is shown in Fig. 13. It can be seen that at the low concentration of particles the calculated collisional frequencies by means of DSMC agree with data calculated by Eq. (33). The results, however, show the larger deviations between the presented simulations by DSMC and calculations using Eq. (33) at the high concentration of particles. The most probable reason could be that the individual particle velocity distribution function is assumed an isotropic Maxwellian distribution in the derivation of Eq. (33). Hence, to gain more insight into the effect of concentration of particles on the collisional behavior, it seems worthwhile to modify the presented sampling method considering the effect of the local distribution of particles, which will be a subject of future research.

To obtain quantitative characterization of cluster flow in a riser, one first needs a systematic criterion for identification of clusters. Soong et al. [41] proposed the following three necessary guidelines. (1) The solid concentration in a cluster must be significantly above the time-average solid concentration at the given local position and operating condition. (2) This perturbation in solid concentration due to clusters must be greater than the random background fluctuations of particle concentration. (3) This concentration perturbation should be sensed for sampling volume with characteristic length scale greater than one to two orders of particle diameter. Being consistent with these guidelines, these investigators imposed a criterion that the local instantaneous particle concentration for a cluster must be greater than the time-averaged concentration by at least two times the standard deviation 2σ, seeing Fig. 14. A cluster would thus be identified if the instantaneous particle concentration exceeds this threshold, existing until the particle concentration again drops below this threshold. In the present study, we will use Soong et al.'s [41] criterion to obtain information of clusters. We would like to point out here that the cluster detection criterion described above is reasonable, but also is somewhat arbitrary. Using a different factor to differentiate from background noise, e.g. 3σ would alter the quantitative results to some degree, but would not change the general characteristics of cluster dynamics. The cluster duration time is $\tau_c = T_b - T_a$. The number-averaged duration time is then [41]:

$$\bar{\tau}_c = \sum_{i=1}^{n} \frac{\tau_{ci}}{n} \tag{34}$$

where n is the total number of clusters detected in an simulation period. τ_{ci} is the ith cluster's duration time. The cluster existence time fraction F_c is:

$$F_c = \frac{\bar{\tau}_c}{\tau} \tag{35}$$

where τ is the simulation time within which n clusters are detected. So, the cluster occurrence frequency λ_c can be gotten.

Fig. 15 shows the distribution of existence time fraction of clusters along the height at the superficial gas velocity of 8.0 m/s. The existence time fraction of clusters decreases along the height at the center. But near the walls it almost keeps as a constant. This means that clusters are easily formed at the bottom. The existence time fraction of clusters at the wall region is greater than that in the center. Manyele et al. [42] investigated gas–solid flow in a riser by a reflective-type fiber optic concentration probe. Particles used were FCC catalyst with a mean diameter of 67 μm and a particle density of 1500 kg/m^3. Experimental results by Manyele et al. [42] showed that the existence time fraction of clusters was about 0-10% at the center region and 15–20% near the walls at the superficial gas velocity 5.5–10.0 m/s. Sharma et al.

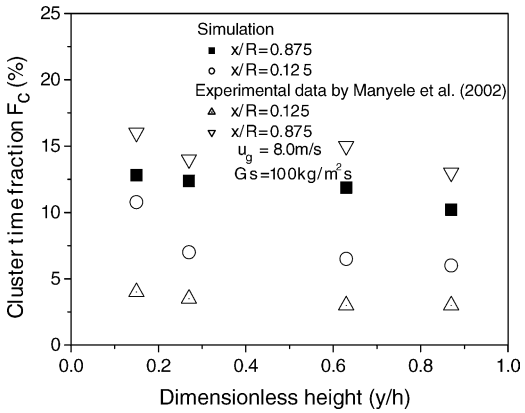

Fig. 15. Time fraction of cluster with bed height.

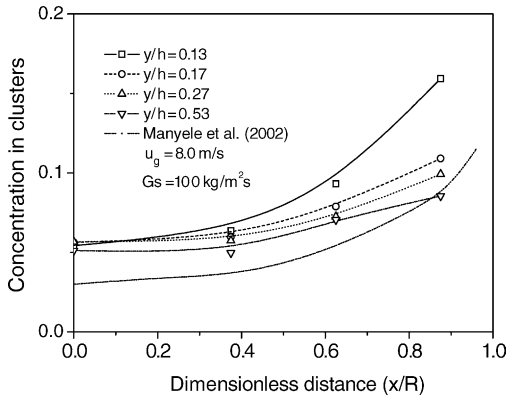

Fig. 17. Mean concentrations in clusters along bed height.

[43] investigated flow behavior of solids in a 15-cm riser by a capacitance-probe measurement of instantaneous local solid concentrations. Particle diameter and density used were 120 μm and 2400 kg/m^3, respectively. Experimental results by Sharma et al. [43] indicated that the existence time fraction of clusters was about 15–20% at the center in the superficial gas velocity of 4.0–6.6 m/s. In the present simulations, the existence time fraction of clusters is about 7–11% at the center and 13–18% near the walls. We see that the simulated results are in agreement with experimental data by Manyele et al. [42] and Sharma et al. [43].

Fig. 16 shows the cluster occurrence frequency at the superficial gas velocity of 8.0 m/s. The cluster occurrence frequency near the walls is greater than that at the center. The simulated results show that the cluster occurrence frequency increases at the bottom due to the effects of gas turbulent flow. We see that the simulated occurrence frequency of clusters is about 3–7 (Hz). Experimental results by Manyele et al. [42] showed that the cluster frequency was 0–10 (Hz) at the center, and 5–20 (Hz) near the walls. Manyele et al. [42] reported that the cluster frequency was 6–12 (Hz) in the riser. Fig. 17 shows the distribution of averaged particle concentration in clusters at the superficial gas velocity of 8.0 m/s. We see that the concentration in cluster is in the range of 0.05–0.1, and decreases along the height near the walls. The particle concentration in clusters near the walls is higher than that at the center. We see that the simulated results are consistent with experiments of Manyele et al. [42].

Helland et al. [44] investigated numerically the gas-particle flow in a vertical two-dimensional circulating fluidized bed using a hard-sphere discrete particles model. The frequency of occurrence, cluster duration time, and time fraction of cluster existence were obtained. Fig. 18 shows the distribution of cluster frequency as a function of superficial gas velocity. Experimental data by Sharma et al. [43] indicated that the cluster frequency varied between 6 and 9 clusters/s. Numerical simulation by Helland et al. [44] shown the cluster frequency varied in the range of 7 and 12 clusters/s. We see that present simulated cluster frequency was lower than that experimental data by Sharma et al. [43] and simulated results by Helland et al. [44]. The trends, however, are the same.

Power spectra density of instantaneous particle concentrations is illustrated in Fig. 19 at the superficial gas velocity of 4.9 m/s by means of Fast Fourier Transform (FFT) method. From the profiles of computed power spectrum density, the frequency domain of particle concentration fluctuations can be determined, which shows the energy distribution

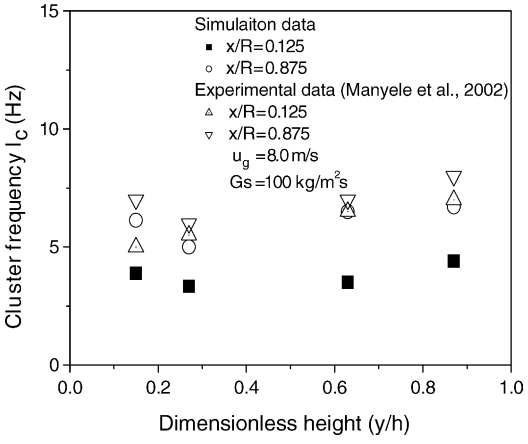

Fig. 16. Cluster frequency along bed height.

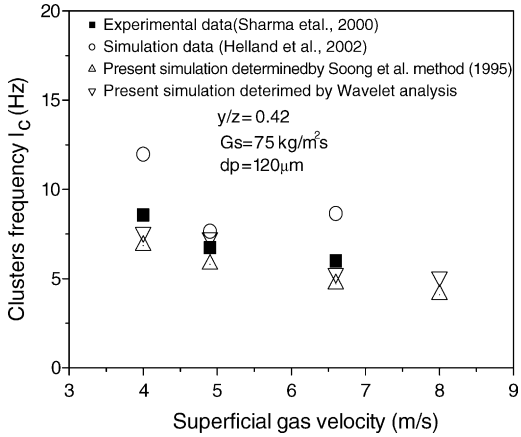

Fig. 18. Profile of cluster frequency as a function of superficial gas velocity.

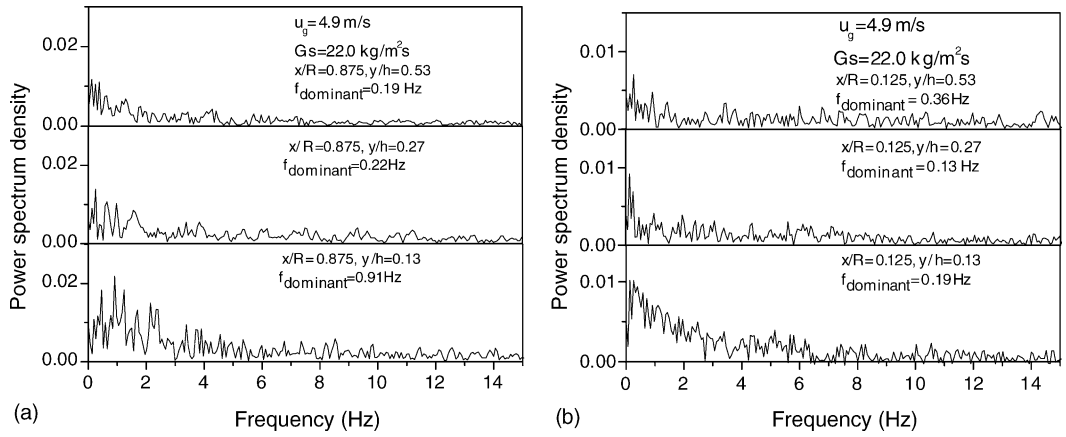

Fig. 19. Power spectrum density of instantaneous particle concentration in the riser.

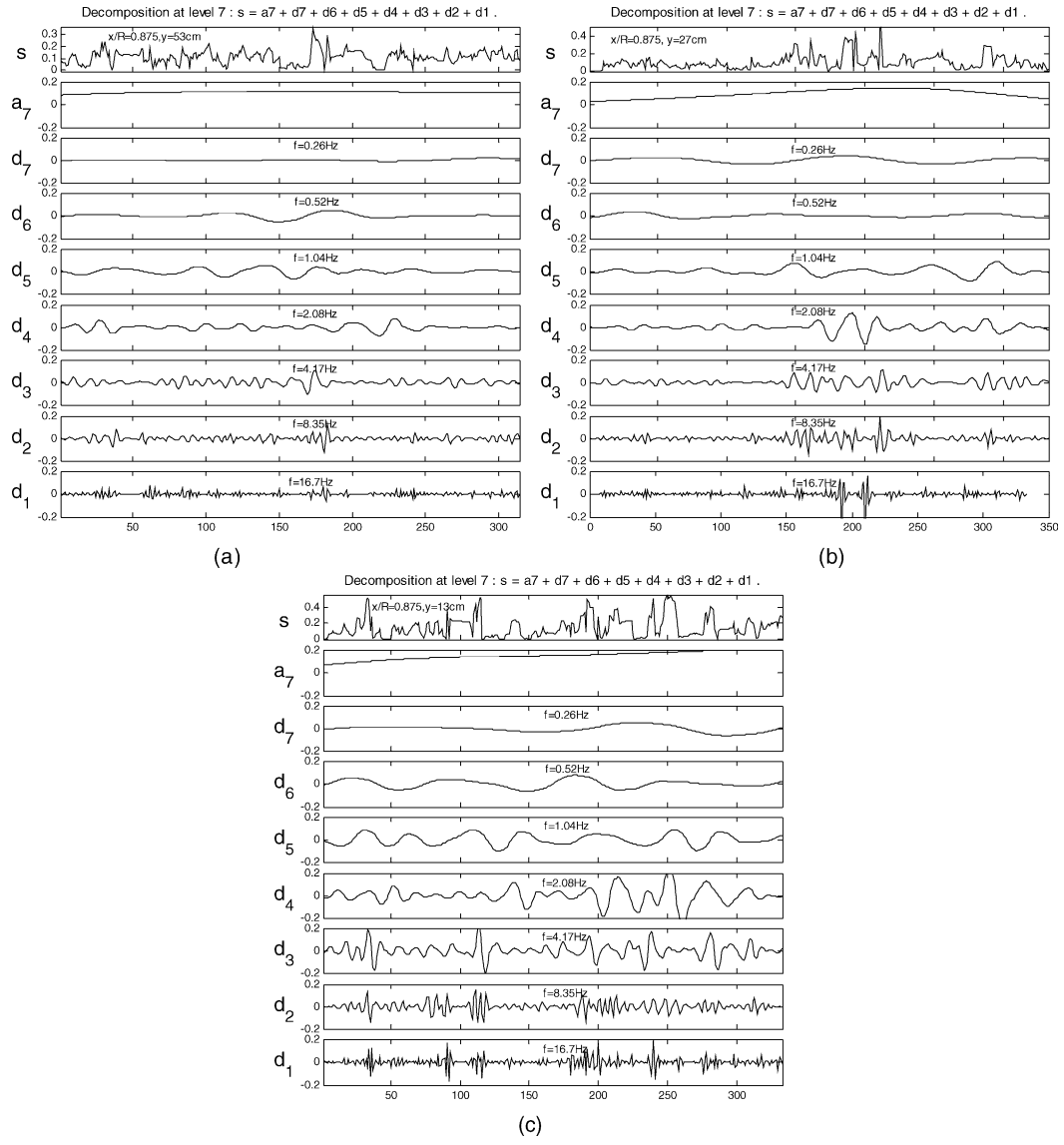

Fig. 20. Wavelet coefficients analysis of fluctuating particle concentration in the riser.

of gas–solid flow in the riser. From these figures, the dominant frequency f_{dominant} can be determined, which corresponds to the highest values of spectra. It is observed that the dominant frequency is in the range of 0.1–1.0 Hz.

Since the hydrodynamics of gas–solid flow in the riser are a complicated nonlinear dynamical system, a detailed understanding of the flow behavior of gas and particles is important. In order to reveal the non-linear dynamical characteristics of gas–solid flow, the wavelet transform (WT) and wavelet multi-resolution analysis can be used. Wavelet transform is a transformation of information from a fine scale to a coarser scale by extracting information that describes the fine scale variability (the detail coefficients or wavelet coefficients) and the coarser scale smoothness (the smooth coefficients or mother-function coefficients). The complete wavelet transform is a process from the finest to the coarsest wavelet level (scale). This describes a scale-by-scale extraction of the variability information at each scale [45,46]. A wavelet $H(t)$ (with real values in our case) transforms a time function (signal) $x(t)$ as:

$$\mathrm{WT}(a, b) = |a|^{-0.5} \int x(t) H\left(\frac{t-b}{a}\right) \mathrm{d}t \tag{36}$$

where the two parameters set of functions $H_{a,b}(t)$ is obtained from a single one, $H(t)$, called the basic (mother) wavelet, through delations by the factor (a) and translations by the factor (b). The factor $|a|^{-0.5}$ is used for normalization purposes whereby all the wavelets in the generated family have the same energy. Eq. (36) implies that the WT can be thought of as a convolution of a function (signal) $x(t)$ with an analysis window $H(t)$ (mother wavelet) shifted in time by (b) and dilated by a scale parameter (a). Each wavelet is located at a different position along the time axis; also each wavelet is localized in the sense that it decreases rapidly to zero when sufficiently far from its center. The scale parameter (a), which can take any value on the positive real axis, is usually chosen such that it is inversely proportional to frequency. Large values of (a) correspond to wide (low frequency) wavelets, while small values of (a) correspond to short (high frequency) wavelets. Thus, by changing the scale parameter (a), while keeping (b) fixed, the wavelet $H_{a,b}(t)$ is allowed to cover the desired frequency range around the time $t = b$. By changing the translation parameter (b) as well one can move the time localization center (b) to the desired position so that at, i.e. $b = b1$, each of the wavelets in the generated family $H_{a,b1}(t)$ is centered around the desired time $t = b1$. The appropriate selection of the two parameters (a) and (b) make the WT extract the localized conditions, i.e. individual (local in time) frequency events of the time varying function (signal) $x(t)$. Different wavelet basis functions will preferentially move, between scales, different characteristics of the target data sets. In this paper, we use the Daubechies family as the wavelet basis function. More details about Daubechies functions can be found in the work of Daubechies [47].

Fig. 20a, b and c show the wavelet multi-resolution analysis of instantaneous particle concentrations at the superficial gas velocity of 4.9 m/s at the three different locations. The time history data of the computed particle concentrations is also plotted in these figures. Through a family of Wavelet filter, a series of detail signals is obtained with different frequency band. Scale 7 signal is the remainder signal by wavelet transform. Hence, the original signal can be reconstructed from the scale 7 signal and other detail signals. They represent the time behavior of the fluctuating particle concentrations within the different frequency bands. The peak of the high frequency component is caused by the turbulence of particle clusters. The signal of dispersed particles is a kind of high frequency quick wave while the particle cluster is a kind of low frequency slow wave. In Fig. 20, it shows the time behavior of the fluctuating particle concentrations within the different frequency bands. The alternative larger positive and negative peaks imply the occurrence of the flow patterns of particle clusters and dispersed particles in the riser. The positive peaks represent the passing of a cluster, and the negative peaks indicate the flow of dispersed particles flow at this moment. Hence, the cluster frequency can be determined from the wavelet multi-resolution analysis. The predicted cluster frequency using the wavelet multi-resolution analysis was shown in Fig. 18. We see that the cluster frequency predicted by wavelet multi-resolution analysis agreed with experimental data. Fig. 21 shows the distribution of cluster frequency at the superficial gas velocity and mass flux of particles of 4.9 m/s and 50 kg/m^2 s in the riser. We see that the cluster frequency is higher near the walls than that at the center, and varies with radial positions in the riser. Making a comparison of the components of concentration fluctuation from the wavelet multi-resolution analysis, it is discovered that alternative large positive and negative peaks appears in the component of 0.52–1.04 Hz to be embedded in the frequency range of original particle concentration fluctuation. These values are coincided with the dominant frequency of 0.1–1.0 Hz from power spectra density distribution in Fig. 16 based on the fast Fourier transfer analysis.

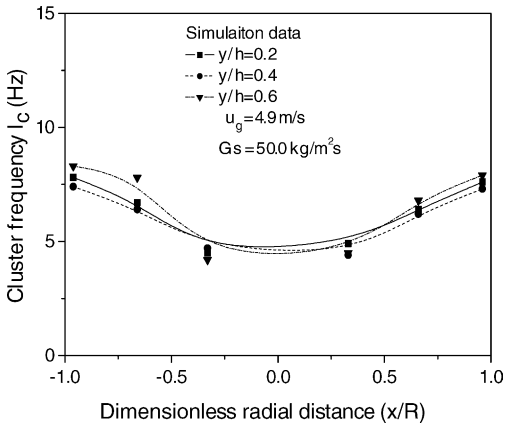

Fig. 21. Distribution of cluster frequency in the riser.

5. Conclusions

Considering the mutual interactions between gas and particles and the particle collisions, the Euler–Lagrangian approach is used to model hydrodynamics of gas and particles phases in the circulating fluidized bed. The large eddy simulation is used to model gas turbulence. Particle collision is modeled by means of the direct simulation Monte Carlo (DSMC) method. The Newtonian equations of motion are solved for each simulated particle in the riser. The distributions of velocity and concentration of particles in the riser were analyzed. The calculated duration time, averaged solid concentration in cluster, the ratio of total cluster duration time to total observation time and the cluster frequency show a reasonable agreement with previous experimental findings. Simulation results show that the particles in the dilute phase exist individually, while the particles in the cluster phase agglomerate with each other and are enmeshed to give irregular shapes and different sizes. The power spectrum of the fluctuations of particle concentration shows that the dominant frequency is in the range from 0.1 to 1.0 Hz. The wavelet analysis method shows that the signal of motion of dispersed particles is a kind of high frequency quick wave, while the cluster flow is a kind of low frequency slow wave. The cluster frequency can be determined from wavelet multi-resolution analysis method. Further analytical work is needed to achieve realistic simulations of cluster flow in the three-dimensional circulating fluidized beds.

Acknowledgement

This work was supported by the National Science Foundation in China through grant No. 50376013, and the cooperative project by NSFC-PetroChina Company Limited under grant No. 20490200.

References

[1] J. Ding, D. Gidaspow, Bubbling fluidization model using kinetic theory of granular flow, AIChE J. 36 (1990) 523–538.
[2] J.A.M. Kuipers, K.J. van Duin, F.P.H. van Beckum, W.P.M. van Swaaij, A numerical model of gas-fluidized beds, Chem. Eng. Sci. 51 (1992) 4087–4102.
[3] C.C. Pain, S. Mansoorzadeh, C.R.E. de Oliveira, Study of bubbling and slugging fluidized beds using the two-fluid granular temperature model, Int. J. Multiphase Flow 27 (2001) 527–551.
[4] C. Guenther, M. Syamlal, The effect of numerical diffusion on simulation of isolated bubbles in a gas–solid fluidized bed, Powder Technol. 116 (2001) 142–154.
[5] E. Peirano, V. Delloume, F. Johnsson, B. Leckner, O. Simonin, Numerical simulation of the fluid dynamics of a freely bubbling fluidized bed: influence of the air supply system, Powder Technol. 122 (2002) 69–82.
[6] J.J. Nieuwland, M. van, J.A.M. Sint Annaland, W.P.M. Kuipers, van Swaaij, Hydrodynamic modeling of gas/particle flows in riser reactors, AIChE J. 42 (1996) 1569–1582.
[7] A. Samuelsberg, B.H. Hjertager, Experimental and numerical study of flow patterns in a circulating fluidized bed reactor, Int. J. Multiphase Flow 22 (1996) 575–591.
[8] A. Neri, D. Gidaspow, Riser hydrodynamics: simulation using kinetic theory, AIChE J. 46 (2000) 52–67.
[9] D.Z. Zhang, W.B. VanderHeyden, High-resolution three-dimensional numerical simulation of a circulating fluidized bed, Powder Technol. 116 (2001) 133–141.
[10] S. Benyahia, H. Arastoopour, T.M. Knowlton, Two-dimensional transient numerical simulation of solids and gas flow in the riser section of a circulating fluidized bed, Chem. Eng. Commun. 189 (2002) 510–527.
[11] L. Cabeze-Gomez, M.F. Eduardo, Numerical study on the influence of various physical parameters over the gas–solid two-phase flow in the 2D riser of a circulating fluidized bed, Powder Technol. 132 (2003) 216–225.
[12] L. Huilin, D. Gidaspow, J. Bouillard, L. Wentie, Hydrodynamic simulation of gas–solid flow in a riser using kinetic theory of granular flow, Chem. Eng. J. 95 (2003) 1–13.
[13] J. De Wilde, B.G. Marin, J.G. Heynderickx, The effects of abrupt T-outlets in a riser: 3D simulation using the kinetic theory of granular flow, Chem. Eng. Sci. 58 (2003) 877–885.
[14] B.P.B. Hoomans, J.A.M. Kuipers, W.J.W. Briels, P.M. van Swaaij, Discrete particle simulation of bubble and slug formation in a two-dimensional gas-fluidized bed: a hard-sphere approach, Chem. Eng. Sci. 51 (1996) 99–118.
[15] B.H. Xu, A.B. Yu, Numerical simulation of the gas–solid flow in a fluidized bed by combining discrete particle method with computational fluid dynamics, Chem. Eng. Sci. 52 (1997) 785–809.
[16] J. Ouyang, J. Li, Discrete simulations of heterogeneous structure and dynamic behavior in gas–solid fluidization, Chem. Eng. Sci. (1999) 5427–5440.
[17] E. Helland, R. Occelli, L. Tadrist, Numerical study of cluster formation in a gas-particle circulating fluidized bed, Powder Technol. 110 (2000) 210–221.
[18] B.G.M. van Wachem, J. van der Schaaf, J.C. Schouten, R. Krishna, C.M. van den Bleek, Experimental validation of Lagrangian–Eulerian simulations of fluidized beds, Powder Technol. 116 (2001) 155–165.
[19] K. Kuwagi, T. Mikami, M. Horio, Numerical simulation of metallic solid bridging particles in a fluidized bed at high temperature, Powder Technol. 109 (2000) 27–40.
[20] M.J. Rhodes, X.S. Wang, M. Nquyen, P. Stewart, K. Liffman, Use of discrete element method simulation in studying fluidization characteristics: influence of interparticle force, Chem. Eng. Sci. 56 (2001) 69–76.
[21] D. Rong, T. Mikafumi, M. Horio, Particle and bubble movements around tubes immersed in fluidized beds—a numerical study, Chem. Eng. Sci. 54 (1999) 5737–5754.
[22] Y. Kaneko, S. Takeo, M. Horio, DEM simulation of fluidized beds for gas-phase olefin polymerization, Chem. Eng. Sci. 54 (1999) 5809–5821.
[23] D. Rong, M. Horio, Behavior of particles and bubbles around immersed tubes in a fluidized bed at high temperature and pressure: a DEM simulation, Int. J. Multiphase Flow 27 (2001) 89–105.
[24] G.A. Bird, Molecular Gas Dynamics and the Direct Simulation of Gas Flows, Clarendon Press, Oxford, 1994.
[25] C. Crowe, M. Sommerfeld, T. Tsuji, Multiphase Flows with Droplets and Particles, CRC Press, Boston, 1998.
[26] S. Yonemura, T. Tanaka, Cluster formation in gas–solid flow predicted by DSMC method, Gas-Solid Flows 166 (1993) 303–309.
[27] T. Tanaka, S. Youemura, K. Kiribayashi, Y. Tsuji, Effects of particle properties on the structure of clusters, American Society of Mechanical Engineers, Fluids Eng. Div. 228 (1995) 297–302.
[28] T. Tanaka, S. Yonemura, K. Kiribayashi, Y. Tsuji, Cluster formation and particle-induced instability in gas–solid flows predicted by the DSMC method, Int. J. JSME 39 (1996) 239–245.

[29] Y. Tsuji, T. Tanaka, S. Yonemura, Cluster patterns in circulating fluidized beds predicted by numerical simulation (discrete particle model versus two-fluid model), Powder Technol. 95 (1998) 254–264.
[30] K.D. Seibert, M.A. Burns, Simulation of fluidized beds and other fluid-particle systems using statistical mechanics, AIChE J. 42 (1996) 660–670.
[31] S. Yuu, H. Nishikawa, T. Umekage, Numerical simulation of air and particle motions in group-B particle turbulent fluidized bed, Powder Technol. 118 (2001) 32–44.
[32] S. Chapman, T.G. Cowling, The Mathematical Theory of Non-uniform Gases, second ed., Cambridge University Press, Camdridge, UK, 1961.
[33] R.A. Bagnold, Experiments on a gravity free dispersion of large solid spheres in a Newtonian fluid under shear, in: Proceedings of the Royal Society of London, vol. A225, 1954, pp. 49–63.
[34] D. Gidaspow, Multiphase Flow and Fluidization: Continuum and Kinetic Theory Descriptions, Academic Press, Boston, 1994.
[35] S. Yuu, T. Ueno, T. Umekage, Numerical simulation of the high Reynolds number slit nozzle gas-particle jet using subgrid-scale coupling large eddy simulation., Chem. Eng. Sci. 56 (2001) 4293–4307.
[36] Y.-D. Jun, W. Tabako, Numerical simulation of a dilute particulate flow over tube banks, J. Fluids Eng. 116 (1994) 770–777.
[37] E. Van den Moortel, R. Azario, L. Santini, Tadrist, Experimental analysis of the gas-particle flow in a circulating fluidized bed using a phase Doppler particle analyzer, Chem. Eng. Sci. 53 (1998) 1883–1899.
[38] M. Ito, M. Tsukada, J. Shimamura, M. Horio, Prediction of cluster size and slip velocity in circulating fluidized beds by a DSMC model, in: L.-S. Fan, T.M. Knowlton (Eds.), Fluidization IX, Engineering Foundation Inc., New York, 1998, pp. 525–532.
[39] M. Tsukada, M. Ito, H. Kamiya, M. Horio, Three-dimension imaging of particle clusters in dilute gas–solid suspension flow, Can. J. Chem. Eng. 75 (1997) 466–470.
[40] D. Gidaspow, L. Huilin, Equation of state and radial distribution function of FCC particles in a CFB, AIChE J. 44 (1998) 279.
[41] C.H. Soong, K. Tuzla, J.C. Chen, Experimental determination of clusters size and velocity in circulating fluidized beds, in: J.F. Large, C. Laguerie (Eds.), Fluidization VIII, Engineering Foundation, New York, 1995, pp. 219–227.
[42] S.V. Manyele, J.H. Parssinen, J.X. Zhu, Characterizing particle aggregates in a high-density and high-flux CFB riser, Chem. Eng. J. 88 (2002) 151–161.
[43] A.K. Sharma, K. Tuzla, J. Matsen, J.C. Chen, Parametric effects of particle size and gas velocity on cluster characteristics in fast fluidized beds, Powder Technol. 111 (2000) 114–122.
[44] E. Helland, R. Occelli, L. Tadrist, Computational study of fluctuating motions and cluster structures in gas-particle flows, Int. J. Multiphase Flow 28 (2002) 199–223.
[45] H. Li, Y. Tomita, Characterization of pressure fluctuation in swirling gas–solid two-phase flow in a horizontal pipe, Adv. Powder Technol. 12 (2001) 169–186.
[46] N. Ellis, L.A. Briens, J.R. Grace, H.T. Bi, C.J. Lim, Characterization of dynamic behavior in gas–solid turbulent fluidized bed using chaos and wavelet analyses, Chem. Eng. J. 96 (2003) 105–116.
[47] I. Daubechies, Ten Lectures on Wavelets, Society for Industrial and Applied Mathematics, 1992.